JBMR Plus, 2024, **8**, 1–14
https://doi.org/10.1093/jbmrpl/ziae006
Advance access publication: January 22 2024
Research Article

Glycoproteomic profile of human tissue-nonspecific alkaline phosphatase expressed in osteoblasts

Diana Atanasova[1], Ekaterina Mirgorodskaya[2], Lavanya Moparthi[3,4], Stefan Koch[3,4], Mathias Haarhaus[5], Sonoko Narisawa[6], José Luis Millán[6], Eva Landberg[1], Per Magnusson[1,*]

[1]Department of Clinical Chemistry, and Department of Biomedical and Clinical Sciences, Linköping University, Linköping SE-58185, Sweden
[2]Proteomics Core Facility, Sahlgrenska Academy, University of Gothenburg, Gothenburg SE-41346, Sweden
[3]Wallenberg Centre for Molecular Medicine, Linköping University, Linköping SE-58185, Sweden
[4]Department of Biomedical and Clinical Sciences, Linköping University, Linköping SE-58185, Sweden
[5]Division of Renal Medicine, Department of Clinical Science, Intervention and Technology, Karolinska Institutet, Karolinska University Hospital, Stockholm SE-14186, Sweden
[6]Sanford Children's Health Research Center, Sanford Burnham Prebys Medical Discovery Institute, La Jolla, CA 92037, United States

*Corresponding author: Per Magnusson, Department of Clinical Chemistry, Department of Biomedical and Clinical Sciences, Linköping University, Linköping SE-58185, Sweden (per.magnusson@regionostergotland.se).

Abstract

Tissue-nonspecific alkaline phosphatase (TNALP) is a glycoprotein expressed by osteoblasts that promotes bone mineralization. TNALP catalyzes the hydrolysis of the mineralization inhibitor inorganic pyrophosphate and ATP to provide inorganic phosphate, thus controlling the inorganic pyrophosphate/inorganic phosphate ratio to enable the growth of hydroxyapatite crystals. N-linked glycosylation of TNALP is essential for protein stability and enzymatic activity and is responsible for the presence of different bone isoforms of TNALP associated with functional and clinical differences. The site-specific glycosylation profiles of TNALP are, however, elusive. TNALP has 5 potential N-glycosylation sites located at the asparagine (N) residues 140, 230, 271, 303, and 430. The objective of this study was to reveal the presence and structure of site-specific glycosylation in TNALP expressed in osteoblasts. Calvarial osteoblasts derived from *Alpl*$^{+/-}$ expressing SV40 Large T antigen were transfected with soluble epitope-tagged human TNALP. Purified TNALP was analyzed with a lectin microarray, matrix-assisted laser desorption/ionization-time of flight mass spectrometry, and liquid chromatography with tandem mass spectrometry. The results showed that all sites ($n = 5$) were fully occupied predominantly with complex-type N-glycans. High abundance of galactosylated biantennary N-glycans with various degrees of sialylation was observed on all sites, as well as glycans with no terminal galactose and sialic acid. Furthermore, all sites had core fucosylation except site N271. Modelling of TNALP, with the protein structure prediction software ColabFold, showed possible steric hindrance by the adjacent side chain of W270, which could explain the absence of core fucosylation at N271. These novel findings provide evidence for N-linked glycosylation on all 5 sites of TNALP, as well as core fucosylation on 4 out of 5 sites. We anticipate that this new knowledge can aid in the development of functional and clinical assays specific for the TNALP bone isoforms.

Keywords: alkaline phosphatase, biomineralization, N-linked glycosylation, glycoprotein, bone formation

Lay Summary

Tissue-nonspecific alkaline phosphatase (TNALP) is a protein that plays a key role in bone formation and mineralization. TNALP produced by bone-forming osteoblast cells is known as bone alkaline phosphatase (BALP). Serum BALP is also a clinically important biomarker of bone formation. The biochemical difference between BALP and other sorts of TNALP is how the protein is processed in the cells by a protein modification process known as glycosylation. During glycosylation, different sugar molecules are synthetized and coupled to specific parts of the TNALP sequence, thereby creating a diverse mixture of protein glycoforms with various length of sugar chains. However, the glycosylation structure and site abundance of glycosylation in TNALP are unknown. In this study, we used different techniques to study protein glycosylation of TNALP synthetized by osteoblasts and found that all hypothetical sites of TNALP were fully glycosylated, which has not been demonstrated before. Furthermore, we found that the glycosylated sites had mixtures of different sugar chains, which might lead to the presence of different glycoforms (isoforms) of BALP. Further studies will examine how the observed sugar chains differ between the BALP glycoforms and what functional role they have in bone formation and mineralization.

Received: December 6, 2023. **Revised:** January 10, 2024. **Accepted:** January 11, 2024

Graphical Abstract

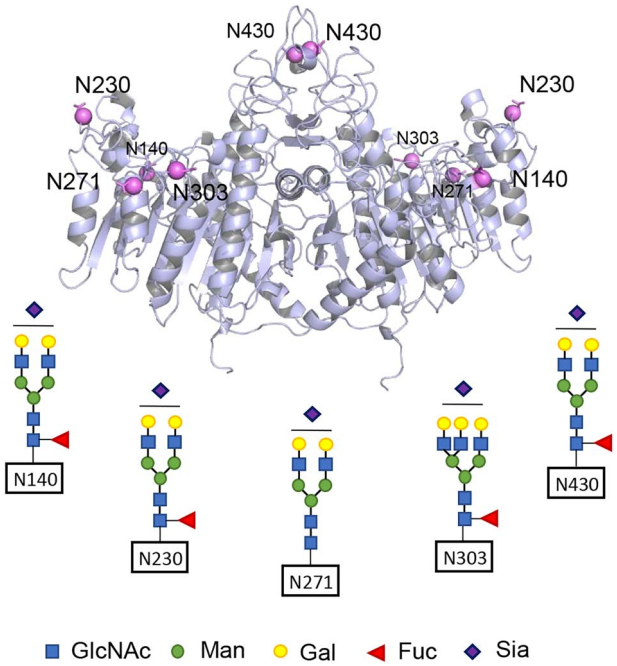

Graphical abstract illustrating the N-glycosylation profile of tissue-nonspecific alkaline phosphatase. The 5 sites N140, N230, N271, N303, and N430 were fully occupied by predominantly biantennary complex-type N-glycans composed of N-acetylglucosamine (GlcNAc), mannose (Man), galactose (Gal), and sialic acid (Sia). Only site N271 did not have core fucose (Fuc).

Introduction

Tissue-nonspecific alkaline phosphatase (TNALP) is part of an evolutionarily conserved isozyme family of alkaline phosphatases (ALP) and comprises about 95% of circulating ALP. TNALP in human serum is predominantly derived from bone and liver sources, in a 1:1 ratio, that can be identified as isoforms identical in protein structure but different in post-translational modifications.[1,2] TNALP is also expressed in other tissues such as the endothelium, kidney, brain, and neutrophil granulocytes.[2]

The human TNALP gene locus, *ALPL*, is located on chromosome 1 p34–p36.1.[3] The over 50 kb-long gene contains 12 exons and encodes a 524-amino-acid long protein, where the first 17 N-terminal amino acids (signal peptide) and the last 22 C-terminal amino acids (pro-peptide) are removed to obtain the mature TNALP protein of 485 amino acids with a molecular weight of 55 kDa.[4] The tertiary structure of TNALP is stabilized by disulfide bonds between 2 identical monomers that contribute to homodimerization.[5,6] TNALP is attached to the outer side of the cell membrane by a glycosylphosphatidylinositol (GPI) anchor and is released by GPI-specific phospholipase D.[2]

In bone, TNALP is expressed by osteoblasts and hypertrophic chondrocytes, and the main functional role for bone ALP (BALP) is to hydrolyze ATP and the potent mineralization inhibitor pyrophosphate to facilitate optimal conditions for local biomineralization.[7] TNALP isolated from the human osteoblastic cell line SaOS-2 comprises 4 glycoforms (BALP isoforms),[8] and the same glycoforms can be detected in the circulation.[1,2] Circulating mouse ALP comprises matching bone glycoforms as observed in humans.[9] Previous studies on lectin precipitation and glycosidase treatment demonstrated that these glycoforms indeed have different N-linked glycosylation patterns.[10,11] Functional studies have shown that these bone glycoforms have different kinetic properties, unique interactions with collagen type I, and vary in their ability to dephosphorylate the mineralization inhibitor osteopontin.[12-14] In addition, these glycoforms differ in their distribution in cortical and trabecular bones[15] and in patients with various metabolic bone diseases.[16-18]

TNALP has 5 potential N-glycosylation sites with canonical consensus sequences NXS/T at 140, 230, 271, 303, and 430, which have been suggested to carry sialylated N-glycans.[8,10] However, the degree of site occupancy and the site-specific glycosylation profiles are yet to be determined.[10,12] N-linked glycosylation is a post-translational modification that is initialized in the endoplasmic reticulum (ER) and proceeds in Golgi apparatus during protein synthesis and is known to affect protein folding, function, transportation, and degradation.[19] Human glycans are mainly composed of N-acetyl glucosamine (GlcNAc), mannose (Man), galactose (Gal), fucose (Fuc), and sialic acid (N-acetylneuraminic acid; Sia), which can be coupled by either α- or β-linkages. N-linked oligosaccharides are initially synthetized and attached to the protein backbone during processing in the ER. These initial structures are composed of 2 GlcNAc residues and one mannose residue, followed by 2 high-mannose branches. Hybrid and complex-type N-glycans are further synthetized in the Golgi by stepwise removal of the high-mannose branch to obtain the core structure of the complex-type N-glycans with 2 GlcNAc and 3 mannose residues. Further processing leads to antenna attachment of one or 2 GlcNAc to each mannose and thereafter potential synthesis of tri- and tetraantennary chains. Terminal sialic acid can be attached to each galactose in α1–3 or α1–6 linkage. Fucose can be attached to galactose by α1–2 linkage or to GlcNAc in α1–3 or α1–4 linkages in the terminal

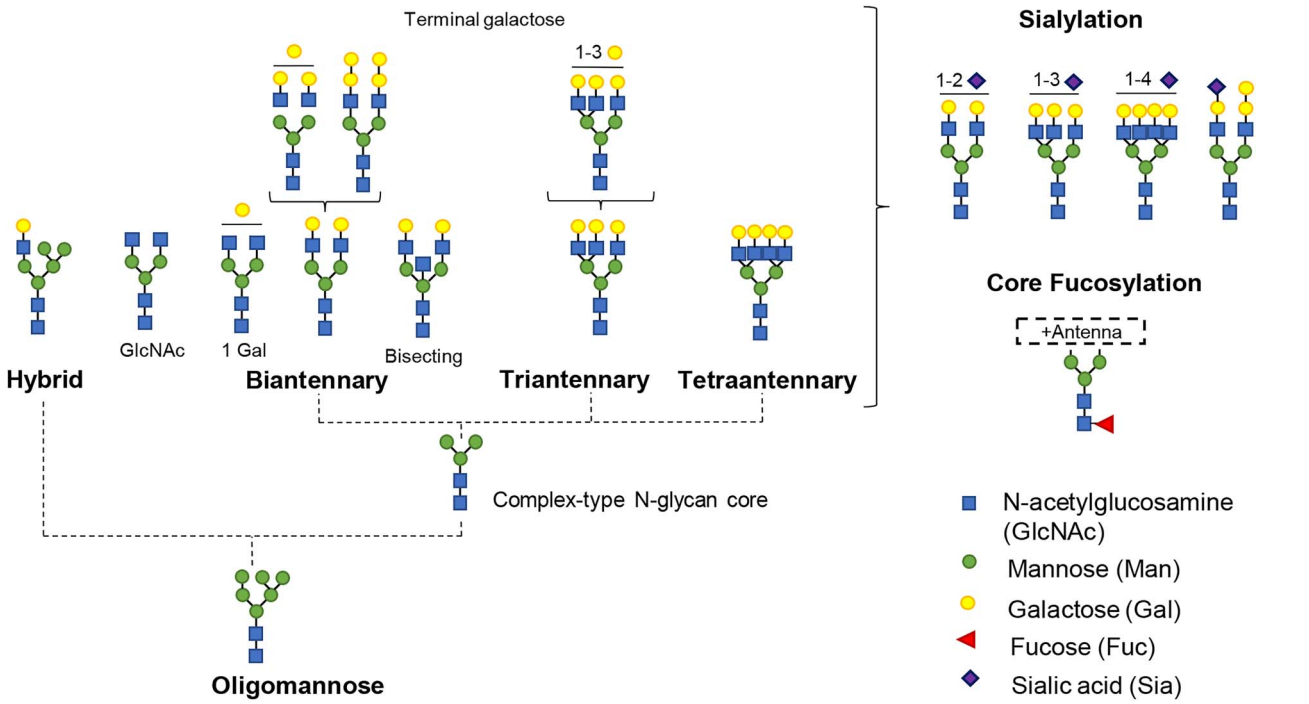

Figure 1. Schematic representation of mammalian complex-type N-glycan synthesis from the high-mannose precursor added in the endoplasmic reticulum and subsequent processing in the Golgi. "+Antenna" = structures above the complex-type N-glycan core, resulting in bi-, tri-, and tetraantennary N-glycans.

part of the structure. Furthermore, fucose in α1–6 linkage can be added to the innermost asparagine-linked GlcNAc, termed core fucosylation (Figure 1).[20]

This study was designed to elucidate the site-specific glycosylation profiles of human TNALP expressed in murine osteoblasts. Human TNALP was expressed from hTNALP-FLAG pcDNA3-vector in *Alpl*$^{+/-}$ mouse calvarial osteoblasts. Soluble epitope-tagged TNALP was purified and analyzed in accordance to the MIRAGE guidelines for glycomic analysis[21,22] by lectin microarray, matrix-assisted laser desorption/ionization-time of flight mass spectrometry (MALDI-TOF MS), and liquid chromatography with tandem mass spectrometry.

Materials and methods

Three-dimensional protein model of TNALP with ColabFold

A 3-dimensional model of TNALP was constructed with ColabFold v1.5.2 that combines the novel DeepMind-based AI database AlphaFold2[23,24] with multiple sequence alignment (MMseq2) extracted from known protein structures in the protein database.[25] In order to obtain the homodimer model of TNALP, an input of the protein sequence (a.a. 18-524, UniProtID: P05186) was inserted in duplicates separated with ":" in the sequence input window at https://colab.research.google.com/github/sokrypton/ColabFold/blob/main/AlphaFold2.ipynb. Multiple sequence alignment (MMSeq2 UniRef+Environmental) in "unpaired+paired" mode was selected to search among structure similarities within and across species, and 3 structure prediction cycles were run with AlphaFold2-multimer-v2. ColabFold then compiles 5 prediction models that are ranked according to the predicted local-distance difference test (pLDDT). All 5 prediction models had high pLDDT scores of >80%. PyMOL v2.5 (Schrödinger) was used to visualize the predicted structure of the TNALP dimer.

Cell culture

Calvarial osteoblasts were isolated from 1-d-old *Alpl*$^{+/-}$ mice following a standard protocol originated form the methods by Boonekamp et al.[26] The isolation procedure is described in detail by Wennberg et al.[27] The procedure was approved by the Institutional Animal Care and Use Committees at Sanford Burnham Prebys Medical Discovery Institute (SBP). The TNAP knockout line has been maintained by *Alpl*$^{+/-}$ heterozygous breeding under specific pathogen-free condition in the vivarium of SBP (currently AUF21-002). SBP animal research program is accredited by the Association for Assessment and Accreditation of Laboratory Animal Care International.

The isolated calvarial osteoblasts were transfected with a pSV3 neo vector and were single-cloned by limiting dilution. Integration of the SV40 Large T antigen gene was confirmed by Southern blot.[28] Clone 2F6 showed mineral deposition when cultured with β-glycerophosphate and ascorbic acid and used in the experiments in this study. Cells were thawed and cultured in Dulbecco's modified Eagles medium (Merck Life Science) supplemented with 10% heat-inactivated fetal bovine serum (Merck Life Science) and 1% Penicillin/Streptomycin (Merck Life Science) in a humidified incubator at 37°C with 5% CO_2. Cells were regularly tested for mycoplasma contamination with Mycoplasma check (Eurofins Analytik GmbH) and were found free from contamination.

Expression and purification of TNALP

The cDNA encoding human TNALP (UniProt: P05186, a.a.1-489) in a pcDNA3 vector was used for expression of human TNALP in mouse osteoblasts. The GPI-anchor gene region was substituted with a FLAG-peptide at the C-terminus

of TNALP to produce secreted epitope-tagged TNALP (*set*TNALP).[29] Mouse osteoblasts were subcultured and transfected using the Nucleofector IIb device with Nucleofector Kit V according to the manufacturer's instructions (Lonza Group). Cells transfected with the *set*TNALP vector, or empty vector, were cultured in Dulbecco's modified Eagles medium with 1% fetal bovine serum and Penicillin/Streptomycin at 37°C/5% CO_2 for 48 h. After incubation, cell medium was collected and concentrated in Vivaspin 20, 30 kDa MWCO filter tubes (Sartorius Group, Göttingen, Germany), and the concentrate was stored at −20°C with EDTA-free protease inhibitor cocktail (ThermoFisher). The expressed *set*TNALP was purified from the concentrated cell medium with FLAG Immunoprecipitation kit (Anti-FLAG M2 Affinity Gel, A2220, Merck Life Science). The protein was eluted with 3X FLAG-peptide (3xDYKDDDDK, Merck Life Science). The protein concentration was measured using a Nanodrop (ThermoFisher) with the molar extinction coefficient of 59.04×1000 M^{-1} cm^{-1} and the theoretical molecular weight for TNALP 54.7 kDa, calculated from the amino acid sequence of TNALP with FLAG-peptide sequence, but without the GPI-anchor signal sequence, in Expasy ProtParam tool (https://web.expasy.org/protparam/). The eluted protein fractions were stored in aliquots in Tris-buffered saline (TBS), pH 7.4 at −20°C until further analysis.

Gel electrophoresis and Western blot

To check the purity of TNALP after immunoprecipitation, 1 μg of eluted protein was denatured and dithiothreitol-reduced in lithium dodecyl sulfate buffer at 80°C for 10 min and separated with SDS-PAGE on a 4%–12% Bis-Tris gel (ThermoFisher). The gel was stained with SilverXpress Silver staining kit (ThermoFisher). Western blot was performed to determine the expression efficiency of TNALP. In brief, protein was transferred to a nitrocellulose membrane, blocked with Intercept TBS buffer (LI-COR Biotechnology GmbH), and incubated with 1:2000 rabbit anti-FLAG monoclonal antibody (F7425, Merck Life Science) in Intercept TBS buffer (LI-COR), 0.1% Tween-20 overnight at 4°C. The membrane was washed with TBST (TBS with 0.1% Tween-20) and incubated with 1:10 000 IRDye 800CW goat anti-rabbit IgG secondary antibody (925–32 213, LI-COR) in Intercept TBS buffer, 0.1% Tween-20 for 1 h at room temperature. The membrane was washed with TBST and developed with Odyssey CLx Imaging System (LI-COR).

Lectin microarray

Purified TNALP was analyzed with the LecChip Lectin Microarray at VelaLabs GmbH (Biomedica Medizinprodukte) according to a standard protocol.[30] In brief, purified TNALP was labeled with Cy3 fluorescent dye, and the free dye was removed by filtering through Zeba Spin desalting columns (ThermoFisher). Serial dilutions (1:1) from 2000 ng/mL to 31.3 ng/mL of Cy3-labeled TNALP were applied on a glass chip with 7 chambers (1 per dilution) with pre-printed lectins. Each chamber contains 45 lectins that are specific for different glycosylation epitopes present on complex-type or high-mannose N-glycans as well as O-type glycans. Lectin origin and specificity are described in Supplementary Table 1. After an overnight incubation at room temperature in a humidity chamber, the level of fluorescence intensity was measured by scanning the LecChip with GlycoStation TM Reader 1200, and the glycoprofile was analyzed with the GlycoStation® Tools Pro Suite 2.0 software (Mx) by normalizing the fluorescent intensity of each lectin to the overall mean intensity of the chip. Results are presented as a heat map with color representation of mean values ($n = 3$) of normalized intensity for each of the 45 lectins in the lectin microarray.

Matrix-assisted laser desorption/ionization-time of flight mass spectrometry

Purified TNALP was dissolved in 0.1 M ammonium bicarbonate, pH 7.8, denatured, and reduced in 0.01% SDS and 0.07% 2-mercapthoethanol at 80°C for 10 min. Glycans were released with 0.06 U PNGase F from *Elizabethkingia meningoseptica* (Merck Life Science) per microgram protein with 10% Triton X-100 for 24 h at 37°C. TNALP not treated with PNGase F was used as control. Denatured PNGase F-treated TNALP was removed with an Isolute C18 column (Biotage) and soluble glycans were collected, desalted with BioGel P-2 gelfiltration (BioRad Laboratories), and vacuum concentrated. Purified glycan samples were derivatized as described by Hronowski et al.[31] by mixing 1:1 with 10 mg/mL 2-anthranillic acid (Merck Life Science) in 90% methanol with 2.5% formic acid and pipetted on a MTP Anchorchip 384 plate. Samples were run on an UltrafleXtreme MALDI-TOF/TOF mass spectrometer (Bruker Corporation) in the negative ion mode. The obtained spectral intensity is derived from an average of 5 high energy analysis (85%) on the crystalized matrix at random positions. Glycans released from transferrin (Merck Life Science) were used as MS calibrator.

Liquid chromatography with tandem mass spectrometry

Purified TNALP preparation (40 μg) in 50 mM triethylammonium bicarbonate, 0.5% sodium deoxycholate, pH 7.4, was reduced with 5 mM dithiothreitol for 30 min at 56°C and alkylated with 10 mM iodoacetamide in the dark for 30 min at room temperature. The alkylation reactions were quenched by incubation with dithiothreitol (10 mM final concentration) for 15 min at room temperature. Prior to proteolytic digest, the alkylated sample was diluted with 50 mM triethylammonium bicarbonate (final volume of 300 μL) and divided into 2 portions for proteolysis using either chymotrypsin (V1061; Promega) (0.3 μg, overnight at 23°C) or with a combination of Lys-C (V1617; Promega) and Glu-C (V1651; Promega) (0.4 μg and 0.3 μg, respectively, overnight at 37°C). Sodium deoxycholate was removed by acidification with 10% trifluoroacetic acid and subsequent centrifugation. Supernatants were further purified using Pierce peptide desalting spin columns (ThermoFisher), according to the manufacturer's instructions. Purified preparations were reconstituted in 2% acetonitrile, 0.1% trifluoroacetic acid for nanoLC–MS/MS analysis. Each of the purified TNALP preparations was divided into 2 equal portions: one half for nanoLC–MS/MS analysis of native sample and the second half for sialidase treatment. For sialic acid removal, TNALP preparations were incubated with 1 μL Sialidase A (GK80040; Agilent Technologies) in 50 μL of provided buffer, overnight at 37°C. All preparations were desalted using Pierce Peptide Desalting Spin Columns (ThermoFisher) prior to LC–MS analysis. The TNALP proteolytic preparations were analyzed on a QExactive HF and an Orbitrap Exploris 480 mass spectrometers interfaced with Easy-nLC1200 liquid chromatography system (ThermoFisher). Peptides were trapped on an Acclaim Pepmap 100 C18 trap column (100 μm × 2 cm, particle size 5 μm; ThermoFisher)

and separated on an in-house packed analytical column (75 μm × 30 cm, particle size 3 μm, Reprosil-Pur C18; Dr Maisch, Ammberbuch-Entringen, Germany) using a gradient from 5% to 35% acetonitrile in 0.2% formic acid over 75 min at a flow of 300 nL/min. Each preparation was analyzed using 2 different MS1 scans settings, in the m/z range of 380–1500 and 600–2000, both at a resolution of 120 K. MS2 analysis was performed in a data-dependent mode at a resolution of 30 K, using a cycle time of 3 s (QExactive HF) or 2 s (Exploris 480). The most abundant precursors with charges 2–7 were selected for fragmentation using higher-energy collisional dissociation (HCD) at collision energy settings of either 28 (QExactive HF) or 30 (Exploris 480). The isolation window was set to either m/z = 1.2 for data acquired in the m/z range of 380–1500 or m/z = 3.0 for data acquired in the m/z range of 600–2000. The dynamic exclusion was set to 10 ppm for 20 s. To facilitate glycosylated peptide characterization, multiple injections were acquired on Exploris 480 with precursors detection in the m/z range of 600–2000 and different settings for the normalized HCD energies of 24, 30, and 38.

Analysis of mass spectrometry data

The acquired data were analyzed using Proteome Discoverer 2.4 (ThermoFisher). Database searches were performed against a custom protein database, consisting of expressed TNALP sequence and the Swiss-Prot *Mus musculus* protein database to control for protein contamination from the production cell-line proteins. The data acquired in m/z range of 380–1500 were searched using Sequest HT. Precursor mass tolerance was set to 5 ppm and fragment mass tolerance to 20 mmu. Chymotryptic peptides with up to 5 missed cleavages and Lys-C/Glu-C peptides with 4 missed cleavages were accepted. Methionine oxidation was set as variable modifications and cysteine alkylation as fixed modifications. Target decoy was used for peptide spectrum match validation.

For glycopeptide analysis, the raw data acquired with different HCD energies were searched using the Byonic software (Protein Metrics, Cupertino) in Proteome Discoverer v2.4, with Minora Feature Detector node, against the single TNALP sequence. Precursor mass tolerance was set to 5 ppm and fragment mass tolerance to 30 ppm. Chymotryptic peptides with 5 missed cleavages and Lys-C/Glu-C peptides with 4 missed cleavages were accepted. In addition to variable N-glycosylation, fixed cysteine alkylation as well as variable methionine oxidation, asparagine deamidation, and amino-terminal pyroglutamic acid formation were allowed. Different N-glycan databases were used during the data processing of native and sialidase-treated samples. Each TNALP proteolytic preparation was analyzed at least 3 times with identical MS1 settings but different fragmentation energies in MS2 to facilitate glycoform identifications. Prior to the final assignment, identified glycosylated peptides were manually validated based on the observed fragmentation pattern, the number of glycoforms per site, the number of peptide spectrum matches per glycoform, and the retention time windows for the different glycoforms (at the same site).The extracted ion chromatogram peak intensities were used to determine the glycoform abundances. The average values from 3 injections were used to calculate glycoform abundances expressed as percent of total signal for all modified and non-modified peptides sharing the same amino acid sequence. These data were used to calculate the glycan distribution at each site. The MS2 data were acquired at different collision energies and were used to evaluate fucose position and antenna compositions including additional Hex presence (HexNAcHexHex). The 26 retrieved and curated non-sialylated compositions were used to create a new glycan database consisting of 72 glycan compositions (both, non-sialylated and sialylated) for the follow-up analysis of native TNALP preparations. The native TNALP proteolytic preparations were then used to evaluate degree of sialylation at each site. The relative glycoform abundances were used to calculate sialylation level for each site. An O-glycan database consisted of 6 O-glycan compositions was used to evaluate the presence of O-glycosylation on TNALP.

Since GlcNAc and GalNAc, as well as galactose and mannose, have the same m/z ratio, they are therefore annotated as N-acetyl hexose (HexNAc) for GlcNAc and GalNAc and hexose (Hex) for galactose and mannose. Deoxyhexose (dHex) is the chemical term for fucose, and neuraminic acid (NeuAc) is for sialic acid. The UniCarb-DB database (https://unicarb-db.expasy.org, accessed March 29, 2023) was used to search for possible N-glycan structures based on the annotations of the chemical terms above. All structures obtained from the mass spectrometry analysis in relation to possible mammalian N-glycan types are presented in Supplementary Table 2.

Results

Potential glycosylation sites of TNAP are located in the peripheral loops

The 3D structure of TNALP, constructed with ColabFold, showed a high prediction score pLDDT >80 (High accuracy pLDDT score 80–100) according to the distance between the residues. The predicted structure of the TNALP dimer is shown in Figure 2A with front and top views. The 5 putative N-glycosylation sites at 140, 230, 271, 303, and 430 are marked on each dimer. All sites with N-glycosylation are located in peripheral loops. The canonical NXS/T sites of TNALP are designated in the amino acid sequence of TNALP in Figure 2B. The GPI-anchor sequence is replaced with FLAG-peptide sequence for the purpose of this study (Figure 2B).

Treatment with N-glycosidase showed that the expressed TNALP is N-glycosylated

Expressed soluble epitope-tagged TNALP, ie, *set*TNALP from mouse osteoblast culture supernatant, was purified with FLAG-immunoprecipitation (FLAG-IP). The degree of purity and specific target enrichment for *set*TNALP was determined by silver staining and Western blot, respectively. This showed a broad band, approximately between 60 and 80 kDa, corresponding to glycosylated TNALP (Figure 3A and B, lane 1), whereas no band was present for the purified sample from cells transfected with pcDNA3-FLAG empty vector (Figure 3A and B, lane 2), indicating the specific isolation of TNALP. Some co-migration of BSA was observed (66 kDa; Figure 3A), and heavy and light chains from FLAG-IP antibody (Figure 3B, lanes 1 and 2) were also detected. PNGase F treatment resulted in one narrow band at approx. 55 kDa, indicating complete digestion of N-linked glycans (Figure 3A and B, lane 3).

Lectin microarray shows presence of complex-type N-glycans, core fucosylation, and sialic acid on TNALP

The relative binding intensity of TNALP to each of the 45 lectins is shown in Figure 4. TNALP showed the highest

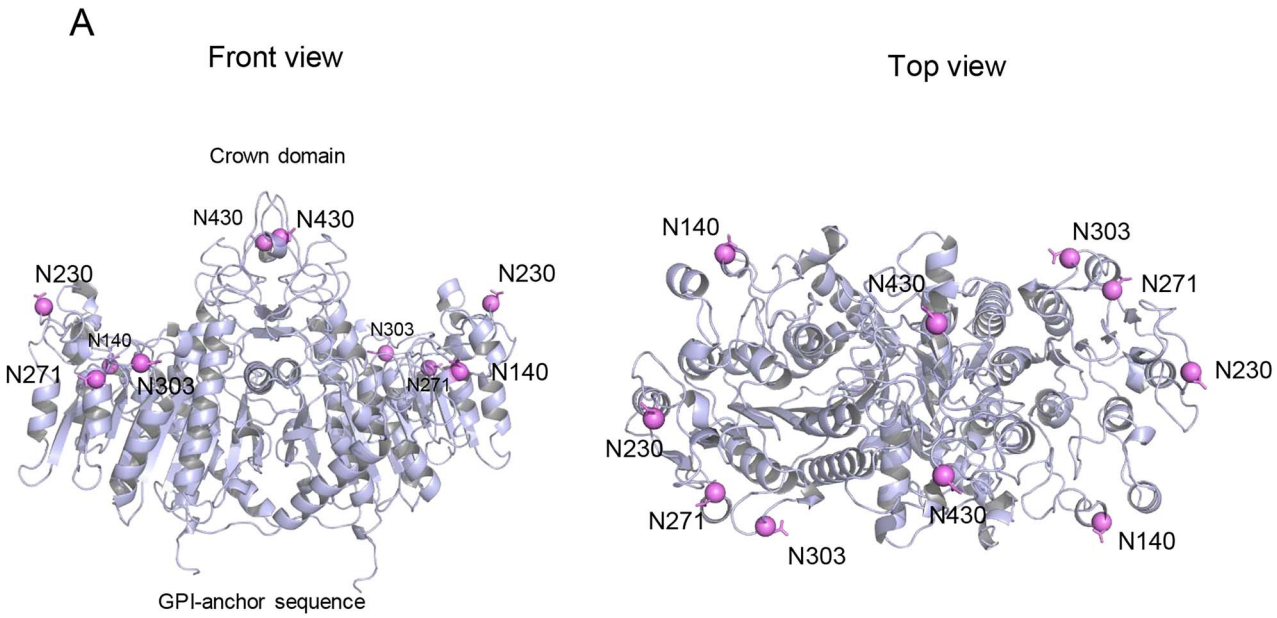

B

```
1   MISPFLVLAIGTCLTNSLVPEKEKDPKYWRDQAQETLKYALELQKLNTNVAKNVIMFLGD 60
61  GMGVSTVTAARILKGQLHHNPGEETRLEMDKFPFVALSKTYNTNAQVPDSAGTATAYLCG 120
121 VKANEGTVGVSAATERSRCNTTQGNEVTSILRWAKDAGKSVGIVTTTRVNHATPSAAYAH 180
181 SADRDWYSDNEMPPEALSQGCKDIAYQLMHNIRDIDVIMGGGRKYMYPKNKTDVEYESDE 240
241 KARGTRLDGLDLVDTWKSFKPRYKHSHFIWNRTELLTLDPHNVDYLLGLFEPGDMQYELN 300
301 RNNVTDPSLSEMVVVAIQILRKNPKGFFLLVEGGRIDHGHHEGKAKQALHEAVEMDRAIG 360
361 QAGSLTSSEDTLTVVTADHSHVFTFGGYTPRGNSIFGLAPMLSDTDKKPFTAILYGNGPG 420
421 YKVVGGERENVSMVDYAHNNYQAQSAVPLRHETHGGEDVAVFSKGPMAHLLHGVHEQNYV 480
481 PHVMAYAACIGANLGHCAPASSAGSL~~AAGPLLLALALYPLSVLF~~(DYKDDDDK)
```

Figure 2. Modeled protein structure of human TNALP (UniProtID: P05186). (A) Three-dimensional structure of the TNALP homodimer and designated location of N-glycosylation sites from front and top view. All 5 N-glycosylation sites are marked with spheres. The protein model was generated with ColabFold (https://colab.research.google.com/github/sokrypton/ColabFold/blob/main/AlphaFold2.ipynb)[25] from the human TNALP amino acid sequence and visualized with PyMOL. (B) Amino acid sequence of a human TNALP monomer. Underlined: pro-peptide sequence (not present in mature form), underlined and bold: possible N-glycosylation motifs at N140, N230, N271, N303, and N430. Crossed out: GPI-anchor signaling peptide, deleted and exchanged with FLAG-peptide sequence (DYKDDDDK) in this study.

signals for lectins with affinity for complex-type N-glycans (DSA, RCA-120, ACG and TxLC-I) including those with terminal galactose (ACG and ABA) and terminal GlcNAc (non-galactosylated glycans; LEL, STL, UDA and WGA), but also complex-type N-glycans with bisecting GlcNAc (PHA(E) and Calsepa). RCA120 and DSA are specific for Galβ1–4GlcNAc structures, present in complex-type N-glycans. ACG had also high affinity for terminally α2–3 sialylated glycans and TxLC-I for core-fucosylated complex-type N-glycans. High signals were also found for lectins specific for terminal sialylation in both Siaα2–3Gal (MAL-I and ACG) and Siaα2–6Gal linkages (SNA, SSA, and TJA-I). Binding to lectins specific for core fucosylation (Fucα1–6GlcNAc; PSA and LCA) but not for terminal fucosylation (Fucα1–2/4Gal; LTL, UAE-I, and AOL) was detected. Low binding signals were mainly observed for O-type lectins, with comparatively higher intensity for lectins specific for Siaα2–3Galβ1–3GalNAc (Jacalin and ACA) and Siaα2–3Galβ1–3(Siaα2–6) GalNAc (MAH).

MALDI-TOF MS: Analysis of released glycans showed presence of biantennary N-glycans with fucose and sialic acid

The N-glycan profile of *set*TNALP was analyzed by MALDI-TOF MS of PNGase F-released glycans (Table 1). MALDI-TOF MS analysis showed presence of glycans in the m/z range of 1500–2900. The calculated 2-aminobenzoic-acid-derivatized masses corresponded to biantennary N-glycan structures with or without fucose and sialic acid. The most abundant structures were biantennary N-glycans with 1 fucose residue and 1 sialic acid (m/z = 2197.071). The majority of the biantennary N-glycans were sialylated (73%). However, impurities of FLAG-peptide used for elution of TNALP during purification were detected at m/z = 2861.9 with high intensity and prevented high quality acquisition of possible triantennary and tetraantennary N-glycans (data not shown).

Table 1. Released N-glycans from TNALP analyzed with MALDI-TOF MS.

Experimental mass (+2-AA) (m/z)	Theoretical mass (+2-AA) (m/z)	Relative intensity (%)[a]	N-Glycan structure
1597.605	1597.42	10 (± 0.1)	Biantennary complex (1 terminal Gal)
1759.725	1759.57	13 (± 1.3)	Biantennary complex (2 terminal Gal)
1905.865	1905.72	5 (± 0.5)	Biantennary complex with 1 fucose
2050.926	2050.83	6 (± 0.1)	Biantennary complex with 1 sialic acid
2197.071	2196.98	62 (± 7.5)	Biantennary complex with 1 fucose and 1 sialic acid
2360.472	2359.13	5 (± 1.9)	Biantennary complex with 1 fucose, 1 sialic acid and 1 extra hexose

[a] Mean ± SD, $n = 3$ Abbreviation: 2-AA, 2-aminobenzoic acid, 119 Da

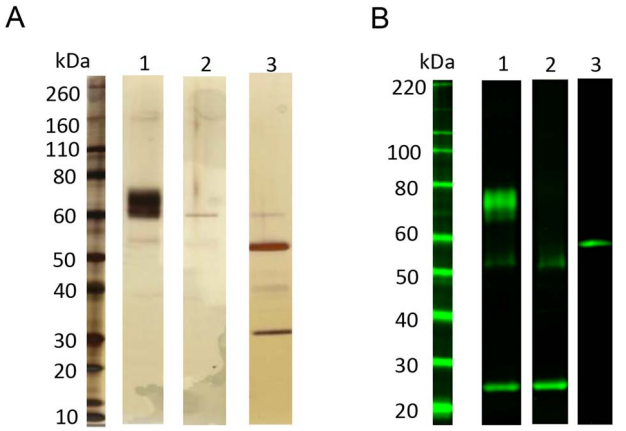

Figure 3. Purified soluble epitope-tagged TNALP (*set*TNALP) expressed in *Alpl*$^{+/-}$ mouse calvarial osteoblasts after FLAG-IP and PNGase F treatment. One microgram of purified *set*TNALP was denatured and loaded on SDS-PAGE and subjected to: (A) silver staining or (B) Western blot. Lane 1: (A and B) *set*TNALP after FLAG-IP. TNALP was detected approximately between 60 and 80 kDa. (B) Presence of heavy (50 kDa) and light (25 kDa) chains from IP antibody. Lane 2: (A and B) Control after FLAG-IP from pcDNA3-FLAG empty vector transfected cells. (A) Presence of BSA (66 kDa). (B) Presences of heavy (50 kDa) and light (25 kDa) chains from IP antibody. Lane 3: (A and B) PNGase F-treated *set*TNALP. Deglycosylated *set*TNALP at approx. 55 kDa, (A) PNGase F at 34 kDa.

LC–MS/MS: All 5 potential sites of TNALP were fully glycosylated

TNALP contains 5 canonical NXS/T N-glycosylation sites. Two different proteolytic preparations, Lys-C plus Glu-C and chymotrypsin, were selected for the analysis of these sites. No glycopeptide enrichment was performed prior to LC–MS/MS, to avoid selective enrichment of specific glycoforms. Instead, to facilitate detection of N-glycopeptides, precursor ions were acquired in the m/z range of 600–2000. Acquired LC–MS/MS data were first evaluated for the occurrence of oxonium ions to confirm the presence of glycopeptides and to estimate their potential glycan compositions. The expected HexNAc, HexNAcHex oxonium ions (m/z = 204 and 365), as well as NeuAc oxonium ions (m/z = 274 and 292) were observed. The mass spectra was also examined for N-glycolylneuraminic acid (NeuGc) oxonium ions (m/z = 290 and 308) as this sialic acid may be present in glycans produced in mouse cells. However, ions consistent with presence of NeuGc were not detected.

The initial proteomics data evaluation confirmed successful TNALP production and purification. Strong signal corresponding to the FLAG-peptide was observed but did not prevent evaluation of the glycosylation sites. The initial data evaluation revealed presence of N-linked glycosylation. Native TNALP preparations were further treated with Sialidase A, prior to the first round of the site-specific glycosylation analysis. Removal of sialic acid decreased site heterogeneity, thus improved the detection of the existing glycoforms and facilitated relative quantification of the site microheterogeneity. To evaluate the presence of O-glycans, both acquisitions (m/z range of 375–1500 and 600–2000) were searched for the presence of the 6 most common human O-glycans. None of these O-glycans were detected.

Table 2. Abundance of N-glycans, core fucose, Galα1–3Gal and sialic acid on TNALP.

	Abundance (%)
High-mannose and hybrid	3
Complex-type:	97
Biantennary	76
Terminal GlcNAc	13
Galactosylated	63
Triantennary	17
Tetraantennary	4
Galα1–3Gal	20
Core fucose	45
1 Sialic acid	21
2 Sialic acids	3
3 Sialic acids	0.04

The extracted ion chromatogram peak intensities were used to determine the glycoform abundances expressed as percent of total signal for all modified and non-modified peptides sharing the same amino acid sequence (described in the *Materials and Methods* section). All 5 putative N-glycosylation sites were occupied to >99% with only minor abundance of the corresponding non-glycosylated peptide in N303 (1%) and N430 (0.2%) (Table 2, Figure 5A). Most of the N-glycans were of the biantennary complex-type (76%). Terminal GlcNAc N-glycans (HexNAc(4)Hex(3)) were present in 13% of all the desialylated glycopeptides. Galactosylated biantennary N-glycans were detected in 63% of the desialylated glycopeptides with 1 or 2 galactose residues (HexNAc(4)Hex(4) or HexNAc(4)Hex(5)). Triantennary N-glycans were detected in 17% of all the desialylated N-glycans, while high-mannose and hybrid glycans and tetraantennary N-glycans were less than 4% abundant on all sites (Table 2, Figure 5A).

The relative abundance of different N-glycans varied among all 5 sites (Figure 5). High-mannose and hybrid N-glycans were present on N271, N303, and N430, while biantennary N-glycans with terminal GlcNAc were present

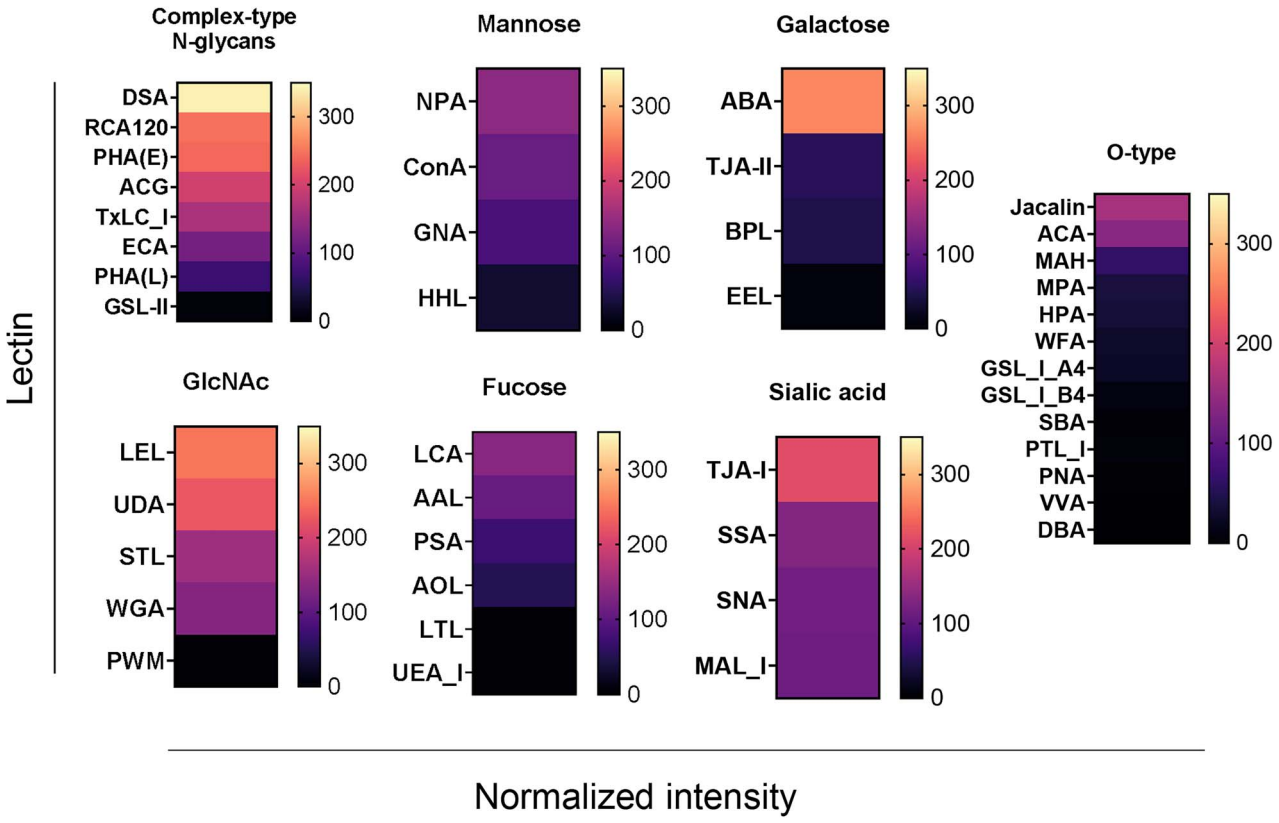

Figure 4. Lectin microarray (LecChip) demonstrating the relative binding of TNALP to different lectins ($n = 45$). Lectin origin and glycan specificity list is presented in Supplementary Table 1. Lectins are grouped according to the nature of their epitopes required for binding to N-glycan epitopes, if not otherwise specified. Lectin microarray analysis was performed with samples from 3 independent expression experiments. Heat map colors represent mean values ($n = 3$) of normalized intensity for each of the 45 lectins in the lectin microarray.

on all sites. Sites N140, N230, N271, and N430 showed the highest abundance of biantennary galactosylated N-glycans, while N303 had the highest abundance of tri- and tetraantennary N-glycans. Tetraantennary N-glycans were only present on N303 and N430 (Figure 5). N140, N230, and N430 had the highest abundance of core-fucosylated biantennary N-glycans (Figure 5). All sites were sialylated with at least 1 sialic acid per complex-type N-glycan (Table 2). Glycans with 2 or 3 sialic acid residues were only found in small amounts with 3% and 0.04% abundance, respectively, and were only present on tri- and tetraantennary N-glycans (Table 2). The highest abundance of sialic acid (29%) was found on triantennary N-glycans (Figure 5C). The highest amount of sialic acid was found on site N271 (32%), while N140, N230, and N430 had a lower degree of sialylation (24%–29%) (Figure 6A). Interestingly, N303 showed the lowest degree of sialylation (4%), despite having a high amount of accessible galactose residues (Figure 6A). Approximately 22% of both bi- and triantennary N-glycans contained an additional fragment ion with strong intensity at m/z 528, corresponding to HexNAcHex (2), which indicates the presence of a galactose extension. The highest amount of galactose extensions was found on site N271 (data not shown). As expected, fragment ions with m/z 657 (HexNAcHexNeuAc) but not m/z 819 (HexNAcHex(2)NeuAc) were found in the mass-spectra of sialylated glycans. This observation suggests a competition of sialyl-transferases and α1–3 galactosyltransferase activity for the same substrate where either sialic acid or galactose will be terminally linked to the GlcNAcβ1–3/4Gal sequence on each antenna.

Although the binding of PHA(E) and Calsepa lectins indicated the presence of bisecting complex-type N-glycans (Figure 4), the typical fragment ions composed of peptide + HexNAc(3)Hex (m/z = peptide +771 m/z)[32] or peptide + HexNAc(3)HexdHex (m/z = peptide +918) were not found in the spectra with low collision energy for any of the 5 sites.

LC–MS/MS: Absence of core fucosylation on N271 possibly due to steric hindrance by W270

The typical fragment ion for core fucose (peptide + HexNAcdHex) at m/z = pept+203 + 146 was observed in 45% of all desialylated glycopeptides (Table 2). Triantennary complex type N-glycans showed higher abundance of core fucose than biantennary glycans (Figure 5B). No terminal fucosylation was observed (HexNAcHexdHex, m/z = 512). Furthermore, the degree of core fucosylation varied among the 5 sites. N140 showed the highest degree of core fucosylation; however, core fucosylation was absent on site N271 (Figure 6B). To determine if there is any connection between the location of N271 and absence of core fucosylation, the 3-dimensional model of TNALP, obtained with ColabFold, was used to measure the proximity of N271 to adjacent amino acids. This revealed that the indol ring of W270 was located approximately 3.8 Å from the free amine side chain of N271, where N-glycosylation occurs, which suggests possible steric hindrance to core fucosylation (Figure 6C).

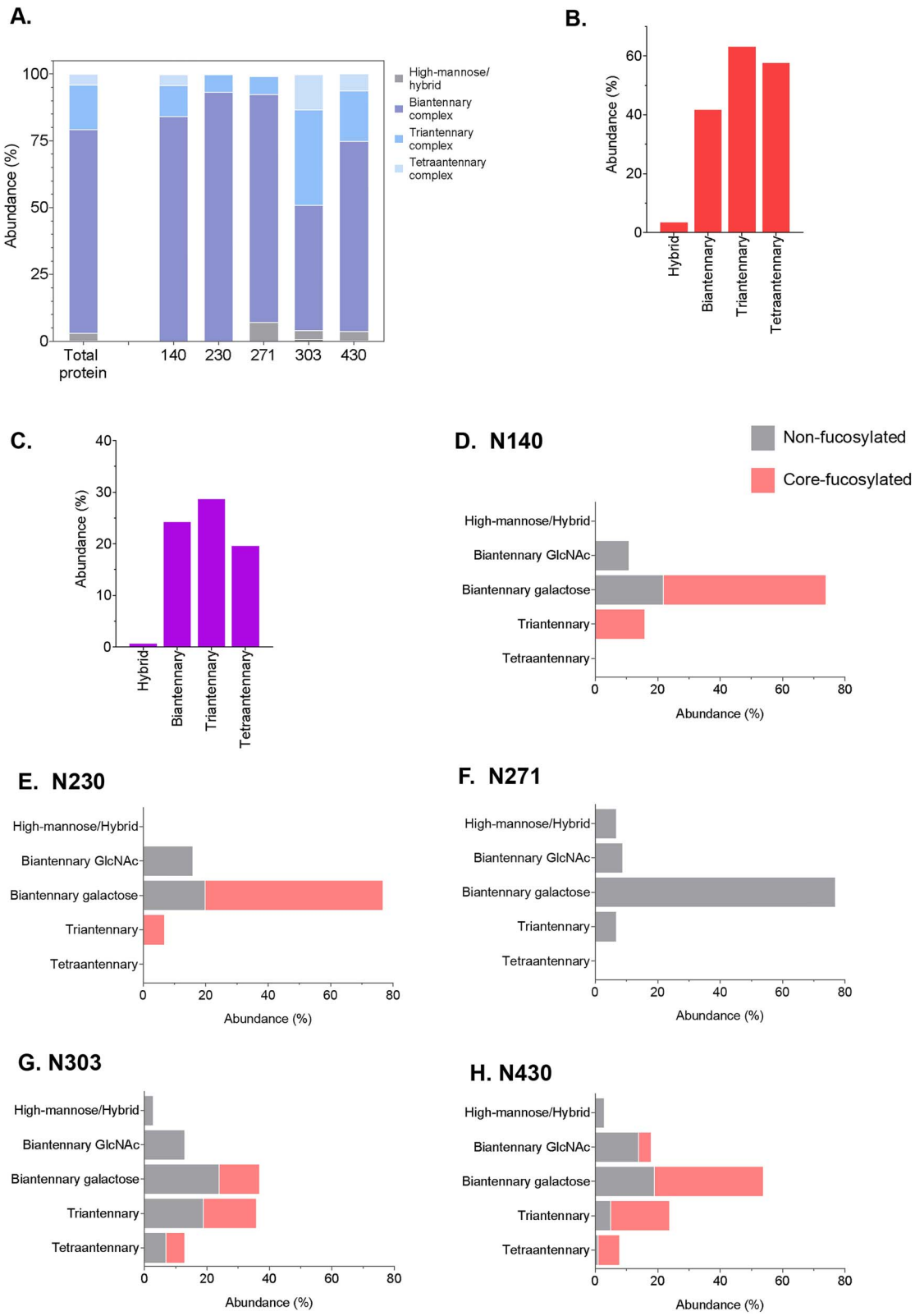

Figure 5. Relative abundance of different N-glycan types on TNALP analyzed with LC–MS/MS analysis. (A) Total glycan abundance on TNALP acquired from desialylated glycopeptides. The highest abundance was observed for biantennary complex-type N-glycans. All 5 sites were fully glycosylated, except N303 that had approximately 1% non-glycosylated peptide. (B) Abundance of core fucosylated N-glycans acquired from desialylated glycopeptides. (C) Abundance of N-glycans with terminal sialic acid acquired from sialylated glycopeptides. (D) N140, (E) N230, (F) N271, (G) N303, and (H) N430. Relative abundance of high-mannose and hybrid and complex-type N-glycans with or without core fucose on the 5 sites of TNALP acquired from LC–MS/MS analysis of desialylated glycopeptides.

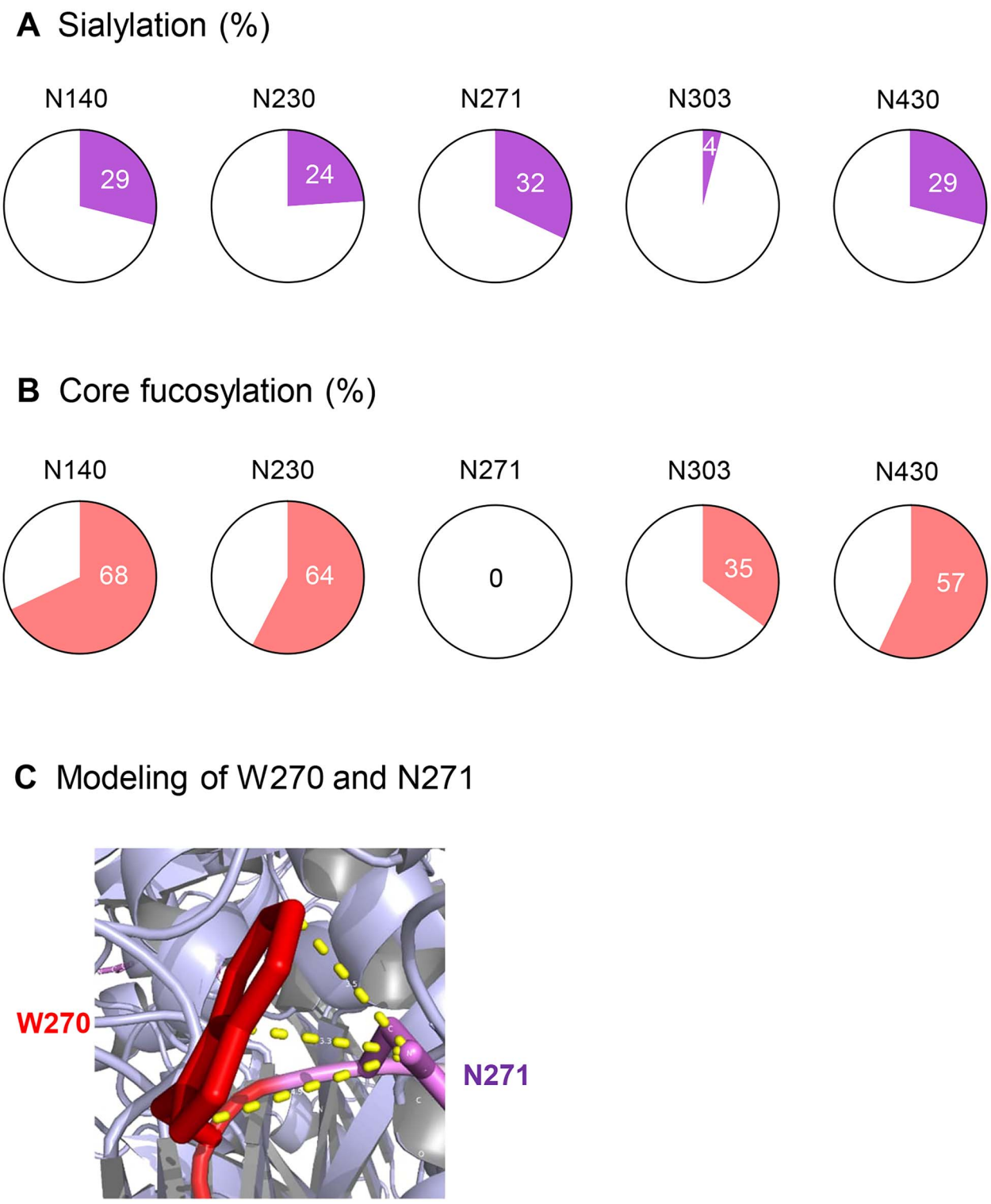

Figure 6. Degree of sialylation and core fucosylation per site. (A) The highest degree of sialylation was observed for N271 and the lowest for N303. (B) The highest degree of fucosylation was observed for N140 and absence of core fucosylation was confirmed for N271. (C) The distance between the indole ring of W270 and the amide group of N271 averages 3.8 Å (dashed lines), measured in PyMOL, suggesting a possible steric hindrance to the amide group and glycosylation site of N271, which might explain the absence of core fucosylation at this site.

Discussion

This is, to our knowledge, the first study that confirms the presence of N-linked glycosylation on all possible 5 N-glycosylation sites of TNALP. We found that most N-glycans were of the biantennary complex type on all sites. Those contained terminal galactose, GlcNAc, or sialic acid in varying amounts. The presence of a high degree of core fucosylated glycans at 4 out of 5 sites was another novel finding. Protein structure prediction using ColabFold revealed that the side chains of the asparagine residues at 140, 230,

271, 303, and 430 are oriented outwards from the main chain, which suggests that all 5 sites are accessible for glycosyltransferases. The modeled TNALP also demonstrated that the N-glycosylation sites were abundant on β-turns and near intermediary unfolded regions, which is known to enhance the folding efficiency and stabilize protein folding by protecting hydrophobic residues to water exposure.[19,20,33] Hence, glycosylation at these structures promotes a higher hydrophilic nature of secreted proteins including TNALP.[19]

The amino acid sequence is a prerequisite for the high degree of glycosylation on TNALP.[20] The most common N-glycan motif on secretory glycoproteins is the NXS/T-motif, where X is any amino acid but proline.[33] The absence of aspartic acid (D), glutamine (Q), tryptophan (W), or leucine (L) at the X-residues of all N-linked sites leads to increased glycosylation efficiency.[19] Early folding events, such as disulfide bonds, might influence the degree of glycosylation at a particular site as the synthetized polypeptide chain enters the ER lumen. The glycan processing rate, protein solubility, and tertiary protein structure influence subsequent glycosylation events such as complex-type N-glycan branching and core fucosylation when the protein is processed through the ER and Golgi.[20] Smaller glycoproteins (544 ± 60 amino acids) are often fully glycosylated by complex-type N-glycans in comparison with larger glycoproteins (896 ± 180 amino acids).[20] We found that TNALP (monomer), composed of 485 amino acids, had 97% complex-type N-glycans fully occupying N140 and N230. Presence of some high-mannose and hybrid glycans at N271, N303, and N430 suggest some incomplete glycosylation processes, or degree of hindrance near these sites, even though N303 also had more tri- and tetraantennary N-glycans in comparison with the other sites. Tri- and tetraantennary N-glycans may be more abundant in β-turn regions with higher accessibility.[20] Taken together, our findings demonstrate that the 5 N-glycan sites of TNALP are highly accessible for glycosylation, and the glycoproteomic analysis with LC–MS/MS confirms that human TNALP is fully glycosylated.

Glycosylation of TNALP has also been proposed as an important factor for normal TNALP function and compartmentalization. Inhibition of N-glycosylation synthesis in osteoblasts led to increased release of TNALP into the osteoblast culture medium and decreased enzymatic activity of membrane–bound TNALP.[34] Furthermore, catalytic activity of both liver- and bone-specific ALP is dependent on the presence of sialic acid.[10-12] PNGase F treatment after desialylation of liver ALP, however, restored the enzymatic activity to native levels.[11] In vivo desialylation of TNALP, using a sialyltransferase-deficient ($ST3Gal6^{-/-}$) mouse model, showed reduced circulating TNALP activity with normal protein expression levels.[35] Sialic acid deficiency enhanced binding of the exposed galactose residues to the Ashwell-Morell receptor in the liver parenchyma, which promotes TNALP uptake and degradation.[35,36]

Lectin microarray and MS analyses of N-glycans on TNALP revealed presence of sialylated complex-type structures. The lectin binding profile showed that sialic acid is present in both α2–3 and α2–6 linkages to Gal. Analyses by MALDI-TOF MS and LC–MS/MS showed mainly monosialylated glycans, but with a significant difference in the degree of sialylation, 73% vs 24%, respectively. This discrepancy reflects probably some loss of sialic acid during sample preparation or ionization in the mass spectrometer. The actual degree of sialylation may therefore be higher than indicated in this study. Although O-linked glycans were not detected by LC–MS/MS analysis, the lectin microarray showed moderate binding to the Jacalin and ACA lectins, which both have affinity to the Sialyl T antigen (Sia α2–3Galβ1–3GalNAcα–). The presence of O-linked glycans on TNALP can therefore not be excluded, and they may contribute to the net charge of TNALP due to additional sialic acid residues.

Core fucosylation is important for protein stability and function.[20] The presence of core fucosylation at 4 out of 5 sites on TNALP is a novel finding in this study. Core fucosylation has previously been reported in placental ALP and ALP from tumorigenic cell lines, such as hepatoma and FL amnion cells.[37-39] Additionally, the lectin microarray analysis in this study showed binding to lectins specific for Fucα1–6GlcNAc (core fucosylation), while there was no binding to lectins specific for terminal fucosylation. According to the LC–MS/MS analysis, the degree of core fucosylation varied among the sites, but no core-fucosylated glycans were found at site N271 and modelling with ColabFold showed possible steric hindrance by W270. Core fucosylation is performed by α1–6 fucosyltransferase (FUT8), which is located in the Golgi and recognizes the NXS/T motif having a higher recognition for complex-type than high-mannose N-glycans.[40] The tertiary structure of the protein determines the accessibility of FUT8, since more buried sites are difficult to access and therefore have a lower degree of core fucosylation.[20] Furthermore, FUT8 is blocked from reaching the N-glycan core by the side chains of proximal amino acids that form a hydrogen bond with functional groups of the innermost GlcNAc.[40] We suggest that W270 induces steric hindrance to N271 in a similar way during the folding of TNALP. Though N271 is efficiently glycosylated, an interaction may occur between the side chain of W270 and the core GlcNAc after glycosylation, which prevents FUT8 interaction with this site. Additional studies are required to determine the role of W270 in the structure and function of TNALP.

TNALP expressed by mesenchymal stem cells has different glycosylation patterns when cultured under either adipogenic or osteogenic conditions, which might influence the localization of TNALP in the cells.[41] We speculate that, during osteoblastogenic differentiation of mesenchymal stem cells, differential glycosylation might lead to the origin of 4 bone-specific glycoforms of TNALP (BALP isoforms). The BALP isoforms B/I, B1, B1x, and B2 are expressed in bone by osteoblasts, and B/I, B1, and B2 are present in serum samples of healthy subjects.[42] The B1x isoform is present in serum only in patients with chronic kidney disease and its detection is associated with lower levels of the other BALP isoforms, total ALP, and with low bone turnover.[43] Calcifying vascular smooth muscle cells demonstrate increased B1x activity and have been proposed as the source of circulating B1x in these patients.[17,44] However, the detection of B1x in serum was associated with better long-term survival,[2] which led to the hypothesis that it may indicate a state of low bone turnover and low BALP associated with improved survival, in accordance with previous reports.[45,46] Despite associations of circulating BALP with several clinically relevant outcomes, it is still unclear whether the circulating BALP isoforms merely reflect tissue activities or whether BALP also is functional in the circulation. More studies are needed to determine how glycosylation affects, and is affected by, the release of

BALP into the circulation and its reactivity toward potential circulating substrates.

The BALP isoforms, in particular B1x, B1, and B2, each have a potential to become biomarkers of clinical use.[1,2,17] However, it is challenging to measure serum BALP due to high antibody cross-reactivity with the liver isoforms, since BALP and liver ALP have identical protein structure.[47,48] Moreover, current immunoassays for the measurement of BALP cannot differentiate between the different BALP isoforms. Therefore, it is of interest to further investigate the post-translational modifications of BALP, in order to develop more specific analytical methods for the BALP isoforms. The development of future isoform-specific detection methods will contribute to the investigations of previously reported differences among these circulating isoforms in metabolic bone diseases.[16-18]

Strengths of the current study include osteoblast-specific protein expression and optimal protein yield needed for accurate glycoproteomic analysis. Moreover, the combined approach of lectin microarray assays and mass spectrometry analysis of both released glycans and glycopeptides provides us with novel and detailed information about the structure of the N-linked glycosylation of TNALP. We selected calvarial osteoblasts from *Alpl*$^{+/-}$ mice as an overexpression system in order to reduce competition with endogenous protein to sugar substrates and glycosyltransferases. Furthermore, this cell line is SV40 T antigen immortalized, which promotes high growth rate and protein yield without changing the primary osteoblastic phenotype.[28] Mouse and human TNALP share 89.9% protein sequence homology and all 5 N-glycan sites are conserved.[9,49] Mouse osteoblasts produce the same BALP isoform pattern as humans and mice have therefore been proposed as a suitable animal model to study the structure and function of TNALP.[2,9] Nonetheless, the choice of a non-human expression model for the study of human TNALP is a limitation since this can potentially influence the glycosylation patterns. For example, we found that some bi- and triantennary N-glycans contained an additional galactose extension, which indicates the presence of Galα1–3Gal epitopes. It is possible that the expression of TNALP in osteoblasts, derived from mouse, has led to Galα1–3Gal expression, an epitope that is highly abundant in many mammalian proteins but absent in humans.[50] This Galα1–3Gal modification might influence the degree of sialylation, as sialylation is hindered at the Galα1–3Gal antenna. It is, however, unknown how this modification influences mouse BALP isoform profile. We found that the isoform profile of the expressed *set*TNALP was similar to the *set*TNALP from the same plasmid in a previous study with human osteoblasts (SaOS-2)[48] and therefore propose that the mouse osteoblasts are a suitable cell model to study the glycosylation of osteoblast-specific TNALP.

In conclusion, we applied an osteoblast-specific expression model for human TNALP and determined the site occupancy and characterized the glycosylation structure of TNALP with a combined computational protein model with a thorough glycomic and glycoproteomic analytical approach. We found that the 5 N-glycan sites located at N140, N230, N271, N303, and N430 were fully occupied by predominantly complex-type N-glycans. Convincing evidence is also presented for a high degree of core fucosylation on N-glycans at all sites, except for site N271, where core fucosylation did not occur. This is presumably due to steric hindrance by W270. Further studies are necessary to explore the functional properties and differences, due to N-linked glycosylation, among the bone-specific isoforms of TNALP driving biomineralization processes.

Acknowledgments

We thank Marcus Roucka, PhD and Sabrina Rottal, MSc at VelaLabs, Vienna, Austria and Gabriela Berg, PhD at Biomedica Medizinprodukte, Vienna, Austria for their expert assistance in lectin microarray analysis and data acquisition. We also thank SciLifeLab and BioMS funded by the Swedish Research Council for providing financial support of the glycoproteomics analysis at the Proteomics Core Facility, Sahlgrenska Academy, Gothenburg, Sweden.

Author contributions

Diana Atanasova (Conceptualization, Data curation, Formal analysis, Investigation, methodology, Project administration, Software, Validation, Visualization, Writing—original draft, Writing—review and editing), Ekaterina Mirgorodskaya (Conceptualization, Data curation, Formal analysis, Investigation, Methodology, Project administration, Resources, Software, Supervision, Validation, Writing—original draft, Writing—review and editing), Lavanya Moparthi (Conceptualization, Formal analysis, Investigation, Methodology, Software, Supervision, Validation, Visualization, Writing—review and editing), Stefan Koch (Conceptualization, Investigation, Methodology, Resources, Writing—review and editing), Mathias Haarhaus (Conceptualization, Investigation, Methodology, Supervision, Writing—review and editing), Sonoko Narisawa (Conceptualization, Methodology, Validation, Writing—review and editing), José Luis Millán (Conceptualization, Methodology, Resources, Validation, Writing—review and editing), Eva Landberg (Conceptualization, Data curation, Formal analysis, Investigation, Methodology, Supervision, Validation, Writing—original draft, Writing—review and editing), and Per Magnusson (Conceptualization, Funding acquisition, Investigation, Methodology, Project administration, Resources, Supervision, Validation, Writing—original draft, Writing—review and editing)

Supplementary material

Supplementary material is available at *JBMR Plus* online.

Funding

This study was supported by grants from the Swedish Research Council, the Swedish Cancer Society, Knut and Alice Wallenberg Foundation, Region Östergötland and Linköping University.

Conflicts of interest

None declared.

Data availability

The data that support the findings of this study are available from the corresponding author upon reasonable request.

References

1. Nizet A, Cavalier E, Stenvinkel P, Haarhaus M, Magnusson P. Bone alkaline phosphatase: an important biomarker in chronic kidney disease – mineral and bone disorder. *Clin Chim Acta*. 2020;501:198–206. https://doi.org/10.1016/j.cca.2019.11.012
2. Haarhaus M, Cianciolo G, Barbuto S, et al. Alkaline phosphatase: an old friend as treatment target for cardiovascular

and mineral bone disorders in chronic kidney disease. *Nutrients*. 2022;14(10):2124. https://doi.org/10.3390/nu14102124
3. Smith M, Weiss MJ, Griffin CA, et al. Regional assignment of the gene for human liver/bone/kidney alkaline phosphatase to chromosome 1p36.1–p34. *Genomics*. 1988;2(2):139–143. https://doi.org/10.1016/0888-7543(88)90095-X
4. Weiss MJ, Henthorn PS, Lafferty MA, Slaughter C, Raducha M, Harris H. Isolation and characterization of cDNA encoding a human liver/bone/kidney-type alkaline phosphatase. *Proc Natl Acad Sci U S A*. 1986;83(19):7182–7186. https://doi.org/10.1073/pnas.83.19.7182
5. Le Du MH, Stigbrand T, Taussig MJ, Menez A, Stura EA. Crystal structure of alkaline phosphatase from human placenta at 1.8 Å resolution - implication for a substrate specificity. *J Biol Chem*. 2001;276(12):9158–9165
6. Mornet E, Stura E, Lia-Baldini AS, Stigbrand T, Ménez A, Le Du MH. Structural evidence for a functional role of human tissue nonspecific alkaline phosphatase in bone mineralization. *J Biol Chem*. 2001;276(33):31171–31178. https://doi.org/10.1074/jbc.M102788200
7. Addison WN, Azari F, Sørensen ES, Kaartinen MT, McKee MD. Pyrophosphate inhibits mineralization of osteoblast cultures by binding to mineral, up-regulating osteopontin, and inhibiting alkaline phosphatase activity. *J Biol Chem*. 2007;282(21):15872–15883. https://doi.org/10.1074/jbc.M701116200
8. Sharp CA, Linder C, Magnusson P. Analysis of human bone alkaline phosphatase isoforms: comparison of isoelectric focusing and ion-exchange high-performance liquid chromatography. *Clin Chim Acta*. 2007;379(1–2):105–112. https://doi.org/10.1016/j.cca.2006.12.024
9. Halling Linder C, Englund UH, Narisawa S, Millán JL, Magnusson P. Isozyme profile and tissue-origin of alkaline phosphatases in mouse serum. *Bone*. 2013;53(2):399–408. https://doi.org/10.1016/j.bone.2012.12.048
10. Magnusson P, Farley JR. Differences in sialic acid residues among bone alkaline phosphatase isoforms: a physical, biochemical, and immunological characterization. *Calcif Tissue Int*. 2002;71(6):508–518. https://doi.org/10.1007/s00223-001-1137-4
11. Komoda T, Sakagishi Y. The function of carbohydrate moiety and alteration of carbohydrate composition in human alkaline phosphatase isoenzymes. *Biochim Biophys Acta*. 1978;523(2):395–406. https://doi.org/10.1016/0005-2744(78)90042-6
12. Halling Linder C, Narisawa S, Millán JL, Magnusson P. Glycosylation differences contribute to distinct catalytic properties among bone alkaline phosphatase isoforms. *Bone*. 2009;45(5):987–993. https://doi.org/10.1016/j.bone.2009.07.009
13. Halling Linder C, Ek-Rylander B, Krumpel M, et al. Bone alkaline phosphatase and tartrate-resistant acid phosphatase: potential co-regulators of bone mineralization. *Calcif Tissue Int*. 2017;101(1):92–101. https://doi.org/10.1007/s00223-017-0259-2
14. Halling Linder C, Enander K, Magnusson P. Glycation contributes to interaction between human bone alkaline phosphatase and collagen type I. *Calcif Tissue Int*. 2016;98(3):284–293. https://doi.org/10.1007/s00223-015-0088-0
15. Magnusson P, Larsson L, Magnusson M, Davie MWJ, Sharp CA. Isoforms of bone alkaline phosphatase: characterization and origin in human trabecular and cortical bone. *J Bone Miner Res*. 1999;14(11):1926–1933. https://doi.org/10.1359/jbmr.1999.14.11.1926
16. Magnusson P, Davie MW, Sharp CA. Circulating and tissue-derived isoforms of bone alkaline phosphatase in Paget's disease of bone. *Scand J Clin Lab Invest*. 2010;70(2):128–135. https://doi.org/10.3109/00365511003642527
17. Haarhaus M, Brandenburg V, Kalantar-Zadeh K, Stenvinkel P, Magnusson P. Alkaline phosphatase: a novel treatment target for cardiovascular disease in CKD. *Nat Rev Nephrol*. 2017;13(7):429–442. https://doi.org/10.1038/nrneph.2017.60
18. Haarhaus M, Fernström A, Qureshi AR, Magnusson P. The novel bone alkaline phosphatase isoform B1x is associated with improved 5-year survival in chronic kidney disease. *Nutrients*. 2021;13(12):4402. https://doi.org/10.3390/nu13124402
19. Esmail S, Manolson MF. Advances in understanding N-glycosylation structure, function, and regulation in health and disease. *Eur J Cell Biol*. 2021;100(7–8):151186. https://doi.org/10.1016/j.ejcb.2021.151186
20. Thaysen-Andersen M, Packer NH. Site-specific glycoproteomics confirms that protein structure dictates formation of N-glycan type, core fucosylation and branching. *Glycobiol*. 2012;22(11):1440–1452. https://doi.org/10.1093/glycob/cws110
21. Struwe WB, Agravat S, Aoki-Kinoshita KF, et al. The minimum information required for a glycomics experiment (MIRAGE) project: sample preparation guidelines for reliable reporting of glycomics datasets. *Glycobiol*. 2016;26(9):907–910. https://doi.org/10.1093/glycob/cww082
22. Kolarich D, Rapp E, Struwe WB, et al. The minimum information required for a glycomics experiment (MIRAGE) project: improving the standards for reporting mass-spectrometry-based glycoanalytic data. *Mol Cell Proteomics*. 2013;12(4):991–995. https://doi.org/10.1074/mcp.O112.026492
23. Jumper J, Evans R, Pritzel A, et al. Highly accurate protein structure prediction with AlphaFold. *Nature*. 2021;596(7873):583–589. https://doi.org/10.1038/s41586-021-03819-2
24. Varadi M, Anyango S, Deshpande M, et al. AlphaFold protein structure database: massively expanding the structural coverage of protein-sequence space with high-accuracy models. *Nucleic Acids Res*. 2022;50(D1):D439–D444. https://doi.org/10.1093/nar/gkab1061
25. Mirdita M, Schütze K, Moriwaki Y, Heo L, Ovchinnikov S, Steinegger M. ColabFold: making protein folding accessible to all. *Nat Methods*. 2022;19(6):679–682. https://doi.org/10.1038/s41592-022-01488-1
26. Boonekamp PM, Hekkelman JW, Hamilton JW, Cohn DV, R.L. J. Effect of culture on the hormone responsiveness of bone cells isolated by an improved sequential digestion procedure. *Proc Kon Ned Akad Wet*. 1984;B87:371–382
27. Wennberg C, Hessle L, Lundberg P, et al. Functional characterization of osteoblasts and osteoclasts from alkaline phosphatase knockout mice. *J Bone Miner Res*. 2000;15(10):1879–1888. https://doi.org/10.1359/jbmr.2000.15.10.1879
28. Chang PL, Gunby JL, Tomkins DJ, Mak I, Rosa NE, Mak S. Transformation of human cultured fibroblasts with plasmids carrying dominant selection markers and immortalizing potential. *Exp Cell Res*. 1986;167(2):407–416. https://doi.org/10.1016/0014-4827(86)90181-3
29. Di Mauro S, Manes T, Hessle L, et al. Kinetic characterization of hypophosphatasia mutations with physiological substrates. *J Bone Miner Res*. 2002;17(8):1383–1391. https://doi.org/10.1359/jbmr.2002.17.8.1383
30. Roucka M, Zimmermann K, Fido M, Nechansky A. Application of lectin array technology for biobetter characterization: its correlation with FcγRIII binding and ADCC. *Microarrays*. 2016;6(1):1. https://doi.org/10.3390/microarrays6010001
31. Hronowski XL, Wang Y, Sosic Z, Wei R. On-MALDI-target N-glycan nonreductive amination by 2-aminobenzoic acid. *Anal Chem*. 2020;92(15):10252–10256. https://doi.org/10.1021/acs.analchem.0c01748
32. Dang L, Shen J, Zhao T, et al. Recognition of bisecting N-glycans on intact glycopeptides by two characteristic ions in tandem mass spectra. *Anal Chem*. 2019;91(9):5478–5482. https://doi.org/10.1021/acs.analchem.8b05639
33. Zielinska DF, Gnad F, Wiśniewski JR, Mann M. Precision mapping of an in vivo N-glycoproteome reveals rigid topological and sequence constraints. *Cell*. 2010;141(5):897–907. https://doi.org/10.1016/j.cell.2010.04.012
34. Farley JR, Magnusson P. Effects of tunicamycin, mannosamine, and other inhibitors of glycoprotein processing on skeletal alkaline phosphatase in human osteoblast-like cells. *Calcif Tissue Int*. 2005;76(1):63–74. https://doi.org/10.1007/s00223-004-0023-2

35. Yang WH, Heithoff DM, Aziz PV, et al. Accelerated aging and clearance of host anti-inflammatory enzymes by discrete pathogens fuels sepsis. *Cell Host Microbe*. 2018;24(4):500–513.e5. https://doi.org/10.1016/j.chom.2018.09.011
36. Ashwell G, Morell AG. The role of surface carbohydrates in the hepatic recognition and transport of circulating glycoproteins. *Adv Enzymol Relat Areas Mol Biol*. 1974;41:99–128
37. Endo T, Ohbayashi H, Hayashi Y, Ikehara Y, Kochibe N, Kobata A. Structural study on the carbohydrate moiety of human placental alkaline phosphatase. *J Biochem*. 1988;103(1):182–187. https://doi.org/10.1093/oxfordjournals.jbchem.a122228
38. Endo T, Higashino K, Hada T, et al. Structures of the asparagine-linked oligosaccharides of an alkaline ahosphatase, Kasahara isozyme, purified from FL amnion cells. *Cancer Res*. 1990;50(4):1079–1084
39. Endo T, Fujiwara T, Ikehara Y, Kobata A. Comparative study of the sugar chains of alkaline phosphatases purified from rat liver and rat AH-130 hepatoma cells. Occurrence of fucosylated high-mannose-type and hybrid-type sugar chains. *Eur J Biochem*. 1996;236(2):579–590. https://doi.org/10.1111/j.1432-1033.1996.t01-1-00579.x
40. García-García A, Serna S, Yang Z, et al. FUT8-directed core fucosylation of N-glycans is regulated by the glycan structure and protein environment. *ACS Catal*. 2021;11(15):9052–9065. https://doi.org/10.1021/acscatal.1c01698
41. Bartlett CL, Ralefatane MG, Cave EM, Crowther NJ, Ferris WF. Differential glycosylation of tissue non-specific alkaline phosphatase in mesenchymal stromal cells differentiated into either an osteoblastic or adipocytic phenotype. *Exp Cell Res*. 2022;421(1):113372. https://doi.org/10.1016/j.yexcr.2022.113372
42. Magnusson P, Sharp CA, Farley JR. Different distributions of human bone alkaline phosphatase isoforms in serum and bone tissue extracts. *Clin Chim Acta*. 2002;325(1–2):59–70. https://doi.org/10.1016/S0009-8981(02)00248-6
43. Haarhaus M, Monier-Faugere MC, Magnusson P, Malluche HH. Bone alkaline phosphatase isoforms in hemodialysis patients with low versus non-low bone turnover: a diagnostic test study. *Am J Kidney Dis*. 2015;66(1):99–105. https://doi.org/10.1053/j.ajkd.2015.02.323
44. Haarhaus M, Arnqvist HJ, Magnusson P. Calcifying human aortic smooth muscle cells express different bone alkaline phosphatase isoforms, including the novel B1x isoform. *J Vasc Res*. 2013;50(2):167–174. https://doi.org/10.1159/000346161
45. Drechsler C, Verduijn M, Pilz S, et al. Bone alkaline phosphatase and mortality in dialysis patients. *Clin J Am Soc Nephrol*. 2011;6(7):1752–1759. https://doi.org/10.2215/CJN.10091110
46. Chen Z, Zhang X, Han F, et al. High alkaline phosphatase and low intact parathyroid hormone associate with worse clinical outcome in peritoneal dialysis patients. *Perit Dial Int*. 2021;41(2):236–243. https://doi.org/10.1177/0896860820918131
47. Broyles DL, Nielsen RG, Bussett EM, et al. Analytical and clinical performance characteristics of Tandem-MP Ostase, a new immunoassay for serum bone alkaline phosphatase. *Clin Chem*. 1998;44(10):2139–2147. https://doi.org/10.1093/clinchem/44.10.2139
48. Magnusson P, Ärlestig L, Paus E, et al. Monoclonal antibodies against tissue-nonspecific alkaline phosphatase. Report of the ISOBM TD9 workshop. *Tumour Biol*. 2002;23(4):228–248. https://doi.org/10.1159/000067254
49. Narisawa S, Harmey D, Magnusson P, Millán JL. Conserved epitopes in human and mouse tissue-nonspecific alkaline phosphatase: second report of the ISOBM TD-9 workshop. *Tumour Biol*. 2005;26(3):113–120. https://doi.org/10.1159/000086482
50. Galili U. Biosynthesis of α-gal epitopes (Galα1-3Galβ1-4GlcNAc-R) and their unique potential in future α-Gal therapies. *Front Mol Biosci*. 2021;8:746883. https://doi.org/10.3389/fmolb.2021.746883